A Pentagon-Proximity Model for Local Aromaticity in Fullerenes and Nanotubes

G. Van Lier,[§] P. W. Fowler,[#] F. De Proft,[§] and P. Geerlings*[,§]

Department of General Chemistry (ALGC), Vrije Universiteit Brussel (VUB), Pleinlaan 2, B-1050 Brussels, Belgium, and School of Chemistry, University of Exeter, Stocker Road, Exeter EX4 4QD, U.K.

Received: September 27, 2001; In Final Form: February 25, 2002

A model is constructed for the local aromaticity of fullerenes and nanotubes. Starting from three infinite series of cylindrical fullerenes, each based on expansion of C_{60} along one of its distinct rotational axes, systematics in global and local aromaticity are derived with simple graph-theoretical methods. Confirmed by ab initio calculations on typical members of each series, these results lead to a general model in which, starting from the positions of the (paratropic) pentagonal rings in the structure, the general pattern of local aromaticity can be constructed, enabling the classification of hexagons by their relative aromaticity. Calculated nucleus-independent chemical shifts (NICS) for fullerene isomers can be rationalized in the new model. In particular, in this pentagon-proximity model, every *leapfrog* fullerene C_{3n} is predicted to have a complete covering by $(n/2 + 2)$ disjoint paratropic rings: the 12 pentagons and those $(n/2 - 10)$ hexagons derived from the parent C_n structure, leaving a connected network of diatropic hexagons everywhere else.

1. Introduction

Because fullerenes are unsaturated carbon systems, it is natural to enquire about their aromaticity. Evidence from chemical properties is against global aromaticity of C_{60} and C_{70}: they behave in many reactions as electron-deficient alkenes.[1−3] The computed magnetic properties of the closed-shell fullerenes are somewhat equivocal. They show overall diamagnetic behavior but with significant variations in local ring currents.[4−9] In the purely magnetic picture, the measure of aromaticity of a ring, and of the local aromaticity of that ring as a component of structure, is its ability to support a diamagnetic (i.e., diatropic) current, and one index of this ability is the nucleus-independent chemical shift or NICS.[10] Here, we treat systematic series of cylindrical fullerenes based on C_{60}, calculate NICS for all rings in a selection of such fullerenes, and show that the results for C_{60} and C_{70} form part of a general pattern, which can be understood using much simpler graph-theory-based arguments in which the variation of local aromaticity in fullerenes is primarily a consequence of the arrangement of the pentagons. In particular, for the class of *leapfrog* fullerenes,[11] C_{3n}, it is predicted that $(n/2-10)$ of the hexagons and all 12 of the pentagons carry paramagnetic local currents (implying positive or small negative NICS values), with diamagnetic circulation in the remaining n hexagons (and thus significantly negative NICS values). The overall magnetic structure can be understood in terms of a mechanical assembly of the counter-rotating rim and hub currents characteristic of circulene systems such as coronene and corannulene.[12]

The structure of the paper is as follows. Section 2 gives computational details. Section 3 reports the results. Section 3.1 gives the construction of three infinite series of cylindrical fullerenes based on expansion of C_{60} along its three distinct rotational axes. Section 3.2 derives systematics in the global aromaticity of these fullerenes from the HOMO−LUMO gaps and analysis of the local aromaticity through ring current calculations. Section 3.3 reports ab initio calculations of global (hardness, magnetizability) and local (NICS) measures of aromaticity for the early members of each series and typical larger cases. Section 3.4 accounts for the NICS values of individual rings in terms of London theory and shows that both the global aromaticity and the pattern of local variation on the fullerene surface can be interpreted with graph-theoretical models. Conclusions are drawn in section 4.

2. Computational Details

Structures were optimized at the AM1 semiempirical level[13] using the MNDO program[14] as a part of the graphical user interface UNICHEM.[15] Global aromaticities were analyzed by considering HOMO−LUMO gaps and molecular magnetizabilities. To investigate local aromaticities, nucleus-independent chemical shifts (NICS) were calculated.[10]

In the first, purely graph-theoretical set of calculations, the molecular graphs of the series of tubular fullerenes treated here were constructed from their face spirals[16] and Hückel energies and vectors calculated by the usual diagonalization of the adjacency matrix. Ring currents were calculated for a number of examples by the Hückel−London method, in which current densities are obtained by diagonalization of a perturbed Hamiltonian matrix.[17,18] The procedure requires as input both the adjacency information and atom coordinates, and the latter are taken directly from the AM1-optimized structures.

For selected examples, ab initio calculations were then performed at the HF/3-21G level using Gaussian 98.[19] HOMO−LUMO gaps were calculated directly from the orbital energies for comparison with the trends deduced from Hückel theory.

* To whom correspondence should be addressed. E-mail: pgeerlin@vub.ac.be.
[§] Vrije Universiteit Brussel (VUB).
[#] University of Exeter.

10.1021/jp013642x CCC: $22.00
Published on Web 04/25/2002

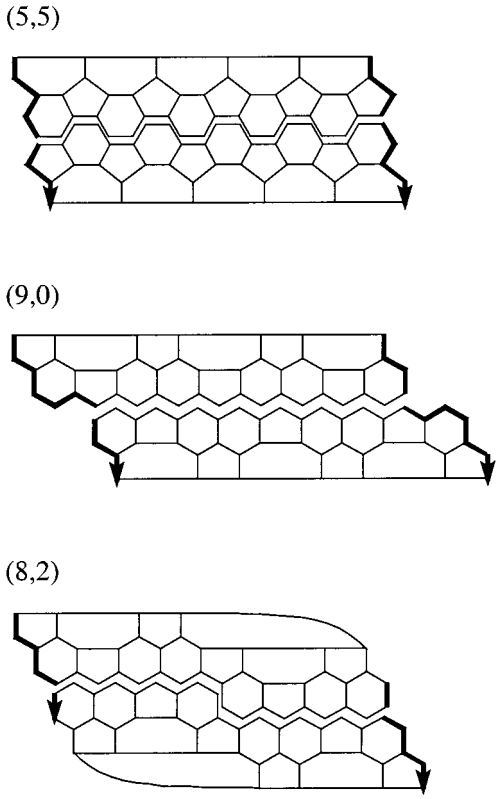

Figure 1. Three ways of cutting C_{60} that retain respectively C_5, C_3, and C_2 axial symmetry and, on extension with a tube of hexagons, lead to (5,5), (9,0), and (8,2) families of capped nanotubes.

NICS values for the five- and six-membered rings were computed at symmetry-distinct ring centers using the GIAO method, and magnetizabilities were evaluated at the same level using the CSGT methodology. (For a review on different methods for analyzing magnetic properties, see ref 20.)

3. Cylindrical Fullerenes

3.1. Construction. The icosahedral C_{60} fullerene molecule has rotational axes of three types: C_5, C_3, and C_2. Each can serve as the basis for construction of an infinite series of cylindrically extended cages, produced by cutting the molecule along an equator and inserting a tubular portion of hexagons.[21−23] In Figure 1, these series are presented in modified Schlegel form, in which the three possible cuts have been shown on the C_{60} diagram and the thick bonds must be superimposed to reconstruct the full three-dimensional structure. The C_5, C_3, and C_2 axes yield armchair, zigzag, and chiral cylinders ("capped nanotubes") of signatures (5,5), (9,0), and (8,2), respectively.[22] These series have provided useful test sets for exploration of electronic structure[24,25,16] and elasticity properties.[26]

The (5,5) series has formula C_{60+10n} with symmetries alternating between D_{5h} ($n = 1, 3, ...$) and D_{5d} ($n = 2, 4, ...$). The (9,0) series has formula C_{60+18n} with a pair of isomers at each n that differ only in the relative orientation of the caps with symmetries D_{3h} and D_3 ($n = 1, 3, ...$) and D_{3d} and D_3 ($n = 2, 4, ...$), respectively. The (8,2) series has formula C_{60+4n} ($n \geq 3$) with symmetry D_{6d} ($n = 3$) and D_2 ($n > 3$) (for $n = 1$ or 2, no isolated pentagon isomer exists[16]). Progression along each of the three series thus adds 5, 9, and 2 hexagons, respectively, for each increase by 1 in n.

3.2. Electronic Structure. Simple Hückel theory predicts a modulation of electronic structure with increasing size along each series. The typical fullerene is electron-deficient and has more formally bonding π orbitals than can be filled by the available electrons;[27] the usual π configuration is "pseudoclosed"[16] with empty bonding orbitals lying above a manifold of doubly occupied orbitals. In contrast, properly closed π configurations, in which all filled orbitals are bonding and all empty orbitals are antibonding, are comparatively rare, and in fact almost all fullerenes of this type fall into one of two systematic classes:[16] the "leapfrogs" and the "carbon cylinders".

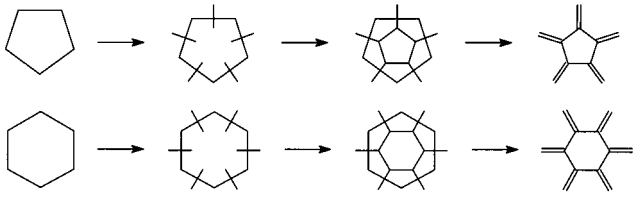

Figure 2. The leapfrog construction. The three-step procedure of crossing, joining, and deleting edges is entirely equivalent to the two-step omnicapping and dualization of a parent fullerene. The transverse edges added in the first step are the formal double bonds in the Fries Kekulé structure for the resulting closed-shell leapfrog fullerene.

The leapfrog closed shells occur at $n = 60 + 6k$ ($k \neq 1$). Leapfrog fullerenes are formally constructed by omnicapping and dualizing smaller fullerenes; thus, to every isomer of the fullerene C_n, there is an equisymmetric leapfrog isomer C_{3n} with isolated pentagons, and this has ($3n$/2) bonding, 0 nonbonding, and ($3n$/2) antibonding π orbitals in the Hückel description.[11,28] Equivalently, the leapfrog can be obtained by crossing all edges of the parent with a new transverse edge, joining the ends of the new edges to make facets within the old faces, and then deleting the parent substructure, as illustrated in Figure 2. Every face of the parent polyhedron gives rise to a similar but rotated face in the product, and all other (hexagonal) faces of the leapfrog arise from vertexes of the parent.

Leapfrog fullerenes have a number of specific combinatorial properties. They are examples of *Clar polyhedra*,[29] in that a disjoint subset of their faces (in this case those derived from the parent) includes all the vertexes exactly once. Each vertex belongs to exactly one such *Clar face*. Two limiting electronic structures match this partition of the faces:[27] *either* all Clar faces carry a mobile sextet of electrons, giving overall a Clar electronic structure appropriate to the 12^- anion, *or* all edges exo to a Clar face are formal double bonds, yielding the Fries Kekule structure of the neutral C_{3n}. In the Fries structure, the maximum possible number of n simultaneously benzenoid hexagons is achieved, and the benzenoid hexagons are exactly those derived from the vertexes of the parent C_n fullerene; each Clar face is then composed entirely of formal single bonds and surrounded by benzenoid hexagons.

The second class of properly closed π shells, the carbon cylinders, consists of cylindrical fullerenes of formula $n = 2p(7 + 3k)$ ($p = 5, 6$; $k = 0, 1, ...$) built by extension of C_{60} either by tubular insertion between two C_{60} caps ($p = 5$) or by expansion of the caps themselves from five- to sixfold symmetry followed by tubular insertion ($p = 6$). The cylinders have (n/2) bonding orbitals lying below an exactly nonbonding LUMO.[24]

The three series of C_{60} expansions contain examples of leapfrogs and carbon cylinders (both $p = 5$ and $p = 6$). Leapfrogs occur for the (5,5) series with $n = 2, 5, 8, ...$, for every achiral member of the (9,0) series, and for the (8,2) series with $n = 0, 3, 6$ .... Closed-shell cylinders occur only for the

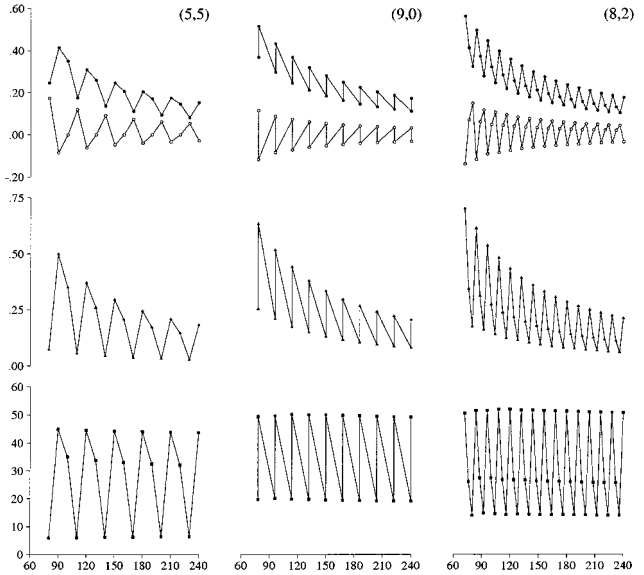

Figure 3. Variation of π-orbital energies, ϵ_{HOMO} (●), ϵ_{LUMO} (○), HOMO−LUMO gap (▲), and kinetic stability parameter T (■) with the number of atoms for the three series of cylindrical fullerenes C_n derived from C_{60} (β units).

(5,5) series with $n = 0, 3, 6, ...$ The sequence of π configurations is therefore predicted to be

for (5,5) A, B, C, A, B, C, ...

for (9,0) C, C, C, ... (achiral)

B, B, B, ... (chiral)

for (8,2) C, B, B, C, B, B, ...

where A is a closed shell with a nonbonding LUMO, B is a pseudoclosed shell, and C is a leapfrog properly closed shell.

3.3. Qualitative Global and Local Aromaticities. The Hückel π orbital energies and gaps (Figure 3) show the periodicity expected from the above discussion, superimposed on the asymptotic trend in which the HOMO, LUMO, and gap would all to tend to zero as n tends to infinity. Because the HOMO−LUMO gap, Δ, is an estimate of the chemical hardness[30] and the latter property has been proposed as a measure of the global aromaticity[31−34,30] (for recent reviews on the use of DFT-based reactivity and stability descriptors, see refs 35−37), the curves in Figure 3 can be interpreted as predicting a similar modulation of global aromaticity, perturbing the general trend to lower hardness and hence lower aromaticity with increasing system size. Specifically, the trends in gap indicate that, in all three series, leapfrogs are more aromatic on this criterion than carbon cylinder isomers, which are in turn more aromatic than the pseudoclosed majority of fullerenes. Most of the size dependence of the HOMO−LUMO gap can be removed by simple multiplication of Δ by the number of conjugated atoms to give the so-called "kinetic stability", T.[38] This quantity was recently found to correlate with the minimum bond resonance energy (min BRE) in a fullerene, and both T and min BRE have been proposed as useful measures for the chemical reactivity of fullerene systems.[38] The kinetic stability gives a clear separation between types A, B, and C, with leapfrogs (C) having $T \approx 45-50$, carbon cylinders (A) having $T \approx 35$, and all others in the set having $T = 27$, in units of the Hückel β parameter.

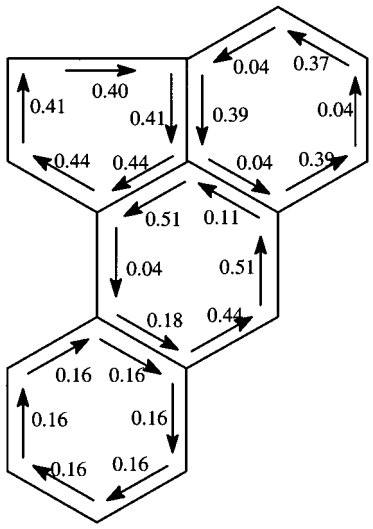

Figure 4. Hückel−London ring currents computed for the D_{6h} isolated-pentagon fullerene C_{72}. This is a composite representation in which each distinct ring is assigned the bond currents calculated for the case when *that ring* is pierced by a perpendicular external magnetic field. The hexagon at bottom left in the diagram has its center on the sixfold axis of the cage. These polar hexagons and the pentagons have continuous paramagnetic ring currents (clockwise in the diagram), whereas the surrounding hexagons (of two symmetry types) have nonuniform diamagnetic circulations.

In addition to its predictions about global aromaticity, Hückel theory can also predict variations in local aromaticity via the simplest treatment of magnetic response, the Hückel−London theory.[39] As a specific example, C_{72} (D_6) is considered here. In the leapfrog construction of C_{72} from the unique C_{24} fullerene, there are exactly 14 faces that originate from the 2 hexagons and 12 pentagons of the C_{24} fullerene parent from which C_{72} is formally derived by leapfrogging. As noted earlier, leapfrog fullerenes have the property that they include the maximum possible number of simultaneously benzenoid hexagons in the Fries Kekule structure. Figure 4 shows the Hückel−London currents computed for each distinct ring of C_{72}, taking the field to be normal to the average plane of the ring in each case. In the Hückel−London model, every all-single bond face of the Fries structure is paratropic and every single−double alternating hexagon is diatropic. Paratropic and diatropic rings are therefore in one-to-one correspondence with the faces and vertexes of the parent from which the leapfrog is derived.

The paratropic character of the rings derived from faces of the parent has a ready interpretation in terms of structural motifs. In the leapfrog, each pentagon becomes the center of a corannulene unit and each face-derived hexagon the center of a coronene unit. In recent ab initio work,[12] a paramagnetic ring current was found for the central (hub) pentagon in corannulene, inducing a counter-rotating diamagnetic ring current along the outer rim. The central current was found to be smaller in the all-hexagon coronene but the global pattern was the same. Both patterns can be explained on the basis of a mechanical analogy—if the central current is strong, it drives currents in its neighbors, which cancel in radial bonds but produce an opposite circulation on the rim. In this way, the central paratropic ring current acts as a motor for the whole pattern. These two examples, and others such as that of kekulene[40] demonstrate the important effect of the countercirculation on inner and outer perimeters of a circumscribing circuit of hexagons. Because the same local patterns are seen in the subunits of C_{72}, this direct calculation of the ring currents with the simple Hückel−London model confirms the relevance of the mechanical analogy.

TABLE 1: HOMO and LUMO Energies, Band Gap, and *T* Value in au Calculated at the ab Initio HF/3-21G Level for Each System[a]

	series	system	symmetry	HOMO energy	LUMO energy	band gap	*T* value
1		C_{60}	I_h	−0.3061	−0.0247	0.2814	16.9
2	(5,5)	C_{70}	D_{5h}	−0.2947	−0.0316	0.2631	18.4
3		C_{80}	D_{5d}	−0.2498	−0.0681	0.1817	14.5
4		C_{90}	D_{5h}	−0.2632	−0.0424	0.2209	19.9
5		C_{150}	D_{5h}	−0.2314	−0.0572	0.1742	26.1
6	(9,0)	C_{78}	D_3	−0.2650	−0.0554	0.2096	16.4
7		C_{78}	D_{3h}	−0.2851	−0.0291	0.2560	20.0
8		C_{96}	D_3	−0.2477	−0.0621	0.1856	17.8
9		C_{96}	D_{3d}	−0.2690	−0.0422	0.2268	21.8
10		C_{150}	D_3	−0.2243	−0.0660	0.1584	23.8
11		C_{150}	D_{3h}	−0.2387	−0.0507	0.1880	28.2
12	(8,2)	C_{72}	D_{6d}	−0.2936	−0.0311	0.2625	18.9
13		C_{76}	D_2	−0.2686	−0.0488	0.2199	16.7
14		C_{80}	D_2	−0.2546	−0.0678	0.1868	14.9
15		C_{84}	D_2	−0.2811	−0.0335	0.2476	20.8
16		C_{88}	D_2	−0.2601	−0.0539	0.2062	18.1
17		C_{92}	D_2	−0.2451	−0.0669	0.1783	16.4
18		C_{100}	D_2	−0.2524	−0.0547	0.1976	19.8
19		C_{144}	D_2	−0.2395	−0.0553	0.1842	26.5
20		C_{148}	D_2	−0.2282	−0.0645	0.1637	24.2
21		C_{152}	D_2	−0.2206	−0.0720	0.1486	22.6

[a] The numbering of structures **1**−**21** is used to give a key to Figure 5.

TABLE 2: Magnetizabilities (in cgs ppm) for the (8,2) Series, Calculated at the ab Initio HF/3-21G Level

system	magnetizabilities
C_{72} (**12**)	−500
C_{76} (**13**)	−539
C_{80} (**14**)	−480
C_{84} (**15**)	−616
C_{88} (**16**)	−671
C_{92} (**17**)	−633
C_{144} (**19**)	−1242
C_{148} (**20**)	−1248
C_{152} (**21**)	−1118

The case of C_{72} will be investigated further with others in the next section in which we move to an ab initio treatment to check the trends in energetic and magnetic properties implied by the mechanical model. To analyze the global aromaticity of the series constructed in 3.1, a number of systems were chosen as further case studies, and their magnetic properties were calculated.

3.4. Ab Initio Studies. Representative members of the three series of expanded C_{60} fullerenes were chosen for further investigation, consisting of the early members of each series and some typical larger cases. For the (5,5) series, the cases treated are C_{70}, C_{80}, C_{90}, and C_{150}, for the (9,0) series C_{78}, C_{96}, and C_{150}, and for the (8,2) series C_{72}−C_{100} and C_{144}−C_{152}. The HOMO−LUMO gap, *T* value, magnetizability, and NICS values were calculated as measures of global and local aromaticity.

Table 1 lists the calculated HOMO and LUMO energies and gaps and the derived *T* values. It can be seen that the periodic variation predicted by Hückel theory survives at the ab initio level. The gaps and *T* values are modulated as predicted. The global aromaticity given by the band gap generally decreases with increasing system size and is indeed correlated with the structure of the molecular graph. In Table 2, magnetizabilities are listed for test cases from the (8,2) series and exhibit a tendency to increase in magnitude with system size. Because magnetizability correlates with the global aromaticity of a system,[30] this trend is to be expected, but the ab initio values also demonstrate a modulation with structure, as predicted by Hückel theory.

As an evaluation of the local aromaticity, Figure 5 shows the NICS values obtained for the various fullerenes. Significant variations are encountered within and between systems. Bearing in mind the NICS values obtained for typical aromatic systems (e.g., −9.9 for benzene at the HF/3-21G level), it is clear that rings in the fullerenes considered here span the range from highly aromatic to antiaromatic.

In Figure 5, all pentagons in the fullerenes considered have positive NICS values and are clearly antiaromatic, with the implication that they are carrying paramagnetic local ring currents. Some hexagons have small NICS magnitudes (∼1 ppm). On the other hand, many six-membered rings have NICS values that nominally represent greater aromaticity than that of benzene itself. It has been suggested that every fullerene has an individual magnetic structure, each case presenting an entirely new problem for ab initio treatment.[9,41] While at some level of detail this must of course be true, several trends are discernible with the help of the graph-theoretical classification, which can be used as the basis of a more detailed interpretation of the NICS distributions in the three series. Especially in cases for which the NICS value is close to the diatropic/paratropic borderline, interpretation of this integral property is materially aided by inspection of the currents themselves.

Taking the NICS maps of Figure 5 for the (8,2) cases as examples, three distinct patterns can be seen, corresponding to the types of electronic configuration predicted in section 3.2: leapfrog closed shell, pseudoclosed shell with medium gap, pseudoclosed with small gap. The standard for comparison is C_{60}, in which the NICS values are 5.1 ppm for pentagons and −6.8 ppm for hexagons calculated in the present approach.

The pattern for the leapfrogs in the (8,2) series (C_{72} (**12**) and C_{84} (**15**)) is that in the leapfrog C_{3n}; the twelve pentagons and the (n/2 − 10) hexagons derived from the parent C_n structure are all paratropic. Pentagon NICS values are +3.3 ppm for C_{72}, and +4.5 to +3.6 ppm for C_{84}. The paratropic hexagons have NICS values of −0.8 ppm in C_{72} and −0.6 ppm in C_{84}. All other hexagons in C_{84} have values in the range −6.6 ppm to −11.4 ppm. In fact, the same pattern can be seen for all of the leapfrog structures in Figure 5 (namely, C_{90} (**4**), C_{78} (**7**) and C_{96} (**9**)) each of which shows a sharp demarcation between the parent-derived rings, with positive NICS, and others (hexagons with NICS < −5.7 ppm).

Turning now to the nonleapfrog cases in the (8,2) series, it is noticeable that these fullerenes have a wider NICS range, with extreme paratropic and diatropic rings but also "intermediate" hexagons. For the nonleapfrog cases with moderate HOMO−LUMO gap in the (8,2) series (C_{76} (**13**) and C_{88} (**16**)), we can see that within the cylinder caps, the C_{60} pattern of paratropic pentagons and diatropic/intermediate hexagons is retained. The bodies of the tubes consist of two intertwined helical strips of hexagons. In C_{76}, C_{88}, ..., the central strips are of length 6, 9, ... The sequences of NICS (ppm) in the strips are

+3.2 (P), −5.2, −13.7, −3.1, −3.1, −13.7, −5.2, +3.2 (P) **(13)**

+4.0 (P), −5.4, −15.0, −4.0, −4.9, −12.2, −4.9, −4.0, −15.0, −5.4, +4.0 (P) **(16)**

so that they carry a strong diatropic NICS on every third

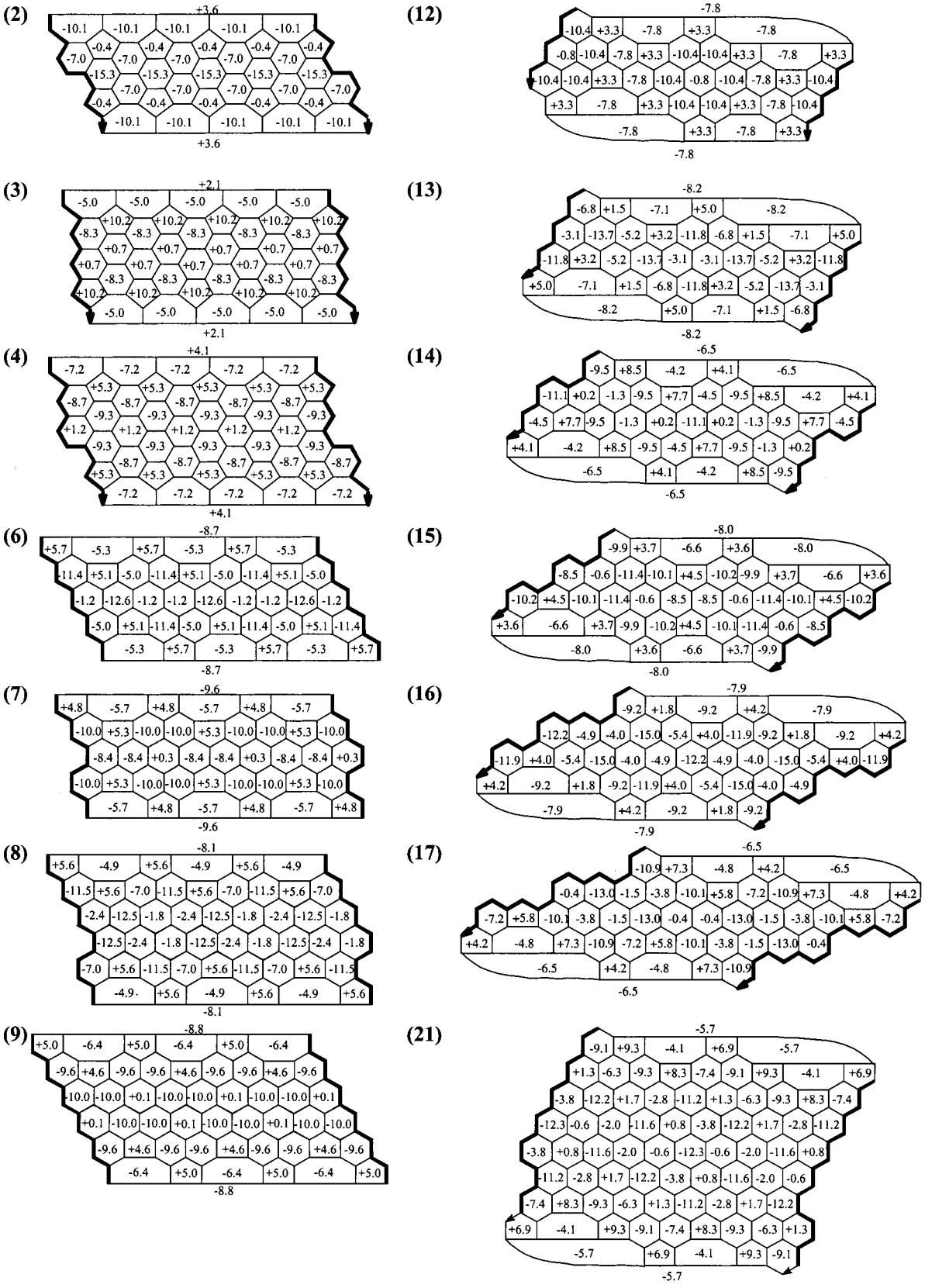

Figure 5. NICS values (ppm) obtained for selected fullerenes C_n in the 3-21G basis at the AM1 geometries. For numbering, see Table 1.

hexagon, starting at one remove from the pentagon, and the general palindromic sequence is

para-P, int-H, dia-H, int-H, ..., int-H, para-P

(para = paratropic, dia = diatropic, int = intermediate, P = pentagon, H = hexagon).

In the small-gap subset (C_{80} (**14**) and C_{92} (**17**)), the NICS distribution in the cap structure is again similar to that in C_{60}

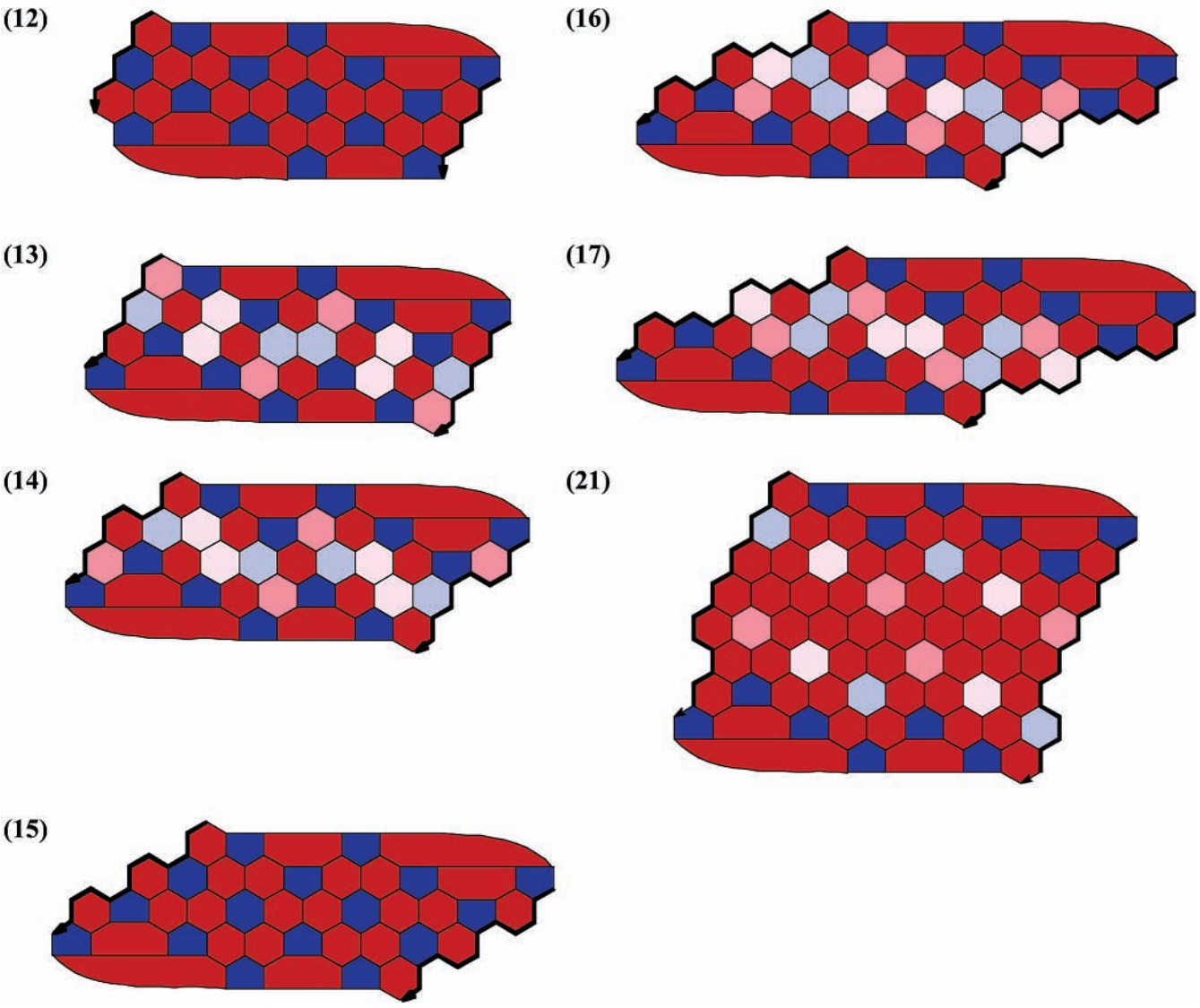

Figure 6. Color-coded maps of the application of the pentagon-proximity model for the (8,2) series: (dark blue ⬟ ⬢) pentagon or hexagon with more than three radiating pentagons; (light blue ⬢) hexagon with three radiating pentagons; (light pink ⬢) hexagon with two radiating pentagons; (dark pink ⬢) hexagon with one radiating pentagon; (red ⬢) hexagon with no radiating pentagons.

and the central hexagonal strips are now of length 7, 10, ... The sequences of NICS (ppm) in the strips are

$$+7.7\ (\mathrm{P}), -9.5, -1.3, +0.2, -11.1, +0.2, -1.3, -9.5, +7.7\ (\mathrm{P}) \qquad (\mathbf{14})$$

$$+5.8\ (\mathrm{P}), -10.1, -3.8, -1.5, -13.0, -0.4, -0.4, -13.0, -1.5, -3.8, -10.1, +5.8\ (\mathrm{P}) \qquad (\mathbf{17})$$

The same palindromic pattern of one diatropic hexagonal ring in three is seen but now with the diamagnetic rings starting from the initial hexagon (the neighbor of a paratropic pentagon) and the intervening hexagons of alternately "intermediate" and paratropic character:

para-P, dia-H, int-H, para-H, ..., int-H, dia-H, para-P.

The next section will present a qualitative model that rationalizes these observations.

3.5. A Model for Local Aromaticity. In section 3.3, it was suggested that the coronene and corannulene motifs provide a mechanical picture of ring-current patterns, with the central paratropic rings acting as motors for the whole pattern. A strong central paratropic circulation will induce diatropic circulations in first neighbors and hence paratropic circulations in neighbors of those neighbors and so on. If a corannulene unit is imagined to be further surrounded with a belt of hexagons (i.e., *circumscribed* in the terminology of Dias[42]), two types of hexagons are added: those with two bonds in common with the corannulene rim and those with one common bond. The mechanical picture suggests that hexagons of the first type should be driven paratropically both by their contacts with the rim and their proximity to the pentagon and those of the second should also be perturbed, but less strongly, from their normal diamagnetism. Further belts of hexagons can be added. The overall effect is then expected to be one of propagation of paratropic character from the central pentagon out to those rings linked to it by exo bonds and then, in larger systems, to the rings linked to them by exo bonds and so on.

Leapfrog fullerenes are exactly matched in structure to the propagation pattern predicted by the mechanical analogy—every parent-derived face is linked by all of its exo bonds to other such faces, so it is possible to establish a self-consistent network

of discrete paratropic rings embedded in a sea of more-or-less diatropic hexagons. This reasoning, applied in section 3.3 to C_{72}, applies to C_{60} itself[6,9] and predicts the properties of the NICS maps for all of the leapfrog structures described in section 3.4 and shown in Figure 5. NICS patterns of general leapfrog fullerenes are amenable to the same analysis, which furthermore rationalizes other known results. The pattern of NICS values for I_h C_{180} shown by Bühl,[9,41] for example, has exactly this interpretation. Of the 80 hexagonal rings in this structure, the 20 at the dodecahedral positions are found to have paratropic NICS values, as have the 12 pentagons. These 32 paratropic rings correspond exactly to the faces derived from the C_{60} parent. All other hexagons are diamagnetic. Bühl's T_d C_{120} isomer is also a leapfrog and shows the same, typical pattern.

Analysis into substructures can also be used to rationalize some of the detail of local aromaticity beyond the simple case of the leapfrog class. Because the paratropic pentagons are taken to dominate the pattern, proximity to a pentagon provides a qualitatitive measure of the local aromaticity of a hexagonal ring. If distance between two rings is defined by the number of bonds in the shortest path between them, then hexagons that have a pentagonal neighbor at distance zero will tend to have enhanced diamagnetism, and hexagons that have one or more pentagons at distance one will tend to have reduced diamagnetism, or even net paramagnetism. A simple classification of the hexagons of a fullerene into those with 0, 1, 2, and 3 or more pentagonal neighbors at distance 1 can account for the main features of the calculated NICS distributions. Figure 6 shows a color coding of the fullerene surface for members of the (8,2) series according to this pentagon-proximity classification. Comparison with the NICS maps of Figure 5 shows, for the leapfrogs C_{72} (**12**) and C_{84} (**15**), perfect agreement on the locations of paratropic and diatropic rings between calculation and the proximity model. For C_{76} (**13**) and C_{88} (**16**), the proximity classification identifies the strongly paratropic and strongly diatropic rings and for the intermediate hexagons it gives the correct ordering of increasing diamagnetism with decreasing pentagon neighbor count. For C_{80} (**14**) and C_{92} (**17**), which are characterized by smaller HOMO−LUMO gap and weaker global aromaticities, the model remains a good guide, picking out the extremes of paramagnetism and diamagnetism, although the NICS ranges of hexagons in the body of the cylinder show some overlap. The same pattern is seen to survive in larger cases, for example, structure **21** in Figure 6.

4. Conclusion

Starting from three infinite series of cylindrical fullerenes, based on the expansion of C_{60} along its distinct rotational axes, aromaticity indicators of a number of fullerenes have been predicted with simple graph-theoretical methods, verified by ab initio calculation. Simple Hückel theory predicts a modulation of the electronic structure, and hence the global aromaticity in each series, superimposed on the general trend to lower aromaticity for increasing system size. By applying recent results for coronene and corannulene to the leapfrog C_{72} fullerene, a model for the local aromaticity of fullerenes and nanotubes has been constructed. Based on the geometrical pattern of the system, a qualitative description of the local aromaticity can be derived from the positions of the pentagons and rationalized in terms of their influence on neighboring rings. In this way, the local magnetic properties of hexagons can be ranked from a simple count of the number of pentagons one bond away. The more such pentagons there are, the smaller the diamagnetic ring current is and the higher the NICS value is to be expected. This essentially graph-theoretical model gives a way of predicting local aromaticity, that is, the pattern of diamagnetic and paramagnetic ring currents, with especially clear results for leapfrog fullerenes, but with general applicability to a broad range of fullerene systems.

References and Notes

(1) Hirsch, A. *The Chemistry of the Fullerenes*; Georg Thieme Verlag: Stuttgart, Germany, 1994.

(2) Taylor, R., Ed. *The Chemistry of Fullerenes*; World Scientific Pub Co: Singapore, 1996.

(3) Taylor, R. *Lecture Notes on Fullerene Chemistry A Handbook for Chemists*; Imperial College Press: London, 1999.

(4) Fowler, P. W.; Lazzeretti, P.; Zanasi, R. *Chem. Phys. Lett.* **1990**, *165*, 79.

(5) Fowler, P. W.; Lazzeretti, P.; Malagoli, M.; Zanasi, R. *Chem. Phys. Lett.* **1991**, *179*, 174.

(6) Haddon, R. C. *Science* **1993**, *261*, 1545.

(7) Haddon, R. C.; Schneemeyer, L. F.; Waszczak, J. V.; Glarum, S. H.; Tycko, R.; Dabbagh, G.; Kortan, A. R.; Muller, A. J.; Mujsce, A. M.; Rosseinsky, M. J.; Zahurak, S. M.; Makhija, A. V.; Thiel, F. A.; Raghavachari, K.; Cockayne, E.; Elser, V. *Nature* **1993**, *350*, 46.

(8) Haddon, R. C.; Pasquarello, A. *Phys. Rev. B* **1994**, *50*, 16459.

(9) Bühl, M. *Chem. Eur. J.* **1998**, *4*, 734.

(10) Schleyer, P. v. R.; Maerker, C.; Dransfeld, A.; Jiao, H.; van Eikema Hommes, N. J. R. *J. Am. Chem. Soc.* **1996**, *118*, 6317.

(11) Fowler, P. W.; Steer, J. I. *J. Chem. Soc., Chem. Commun.* **1987**, 1403.

(12) Steiner, E.; Fowler, P. W.; Jenneskens, L. W. *Angew. Chem., Int. Ed.* **2001**, *40*, 362.

(13) Stewart, J. P. P. *J. Comput.-Aided Mol. Des.* **1990**, *4*, 1.

(14) Dewar, M. J. S.; Thiel, W. *J. Am. Chem. Soc.* **1977**, *99*, 4899.

(15) *UniChem*; Cray Research Inc.: Eagon, MN, 1994.

(16) Fowler, P. W.; Manolopoulos, D. E. *An Atlas of Fullerenes*; Oxford University Press: Oxford, U.K., 1995.

(17) Pasquarello, A.; Schlüter, M.; Haddon, R. C. *Phys. Rev. A* **1993**, *47*, 1783.

(18) Ceulemans, A.; Chibotaru, L. F.; Fowler, P. W. *Phys. Rev. Lett.* **1998**, *80*, 1861.

(19) Frisch, M. J.; Trucks, G. W.; Schlegel, H. B.; Scuseria, G. E.; Robb, M. A.; Cheeseman, J. R.; Zakrzewski, V. G.; Montgomery, J. A., Jr.; Stratmann, R. E.; Burant, J. C.; Dapprich, S.; Millam, J. M.; Daniels, A. D.; Kudin, K. N.; Strain, M. C.; Farkas, O.; Tomasi, J.; Barone, V.; Cossi, M.; Cammi, R.; Mennucci, B.; Pomelli, C.; Adamo, C.; Clifford, S.; Ochterski, J.; Petersson, G. A.; Ayala, P. Y.; Cui, Q.; Morokuma, K.; Malick, D. K.; Rabuck, A. D.; Raghavachari, K.; Foresman, J. B.; Cioslowski, J.; Ortiz, J. V.; Stefanov, B. B.; Liu, G.; Liashenko, A.; Piskorz, P.; Komaromi, I.; Gomperts, R.; Martin, R. L.; Fox, D. J.; Keith, T.; Al-Laham, M. A.; Peng, C. Y.; Nanayakkara, A.; Gonzalez, C.; Challacombe, M.; Gill, P. M. W.; Johnson, B. G.; Chen, W.; Wong, M. W.; Andres, J. L.; Head-Gordon, M.; Replogle, E. S.; Pople, J. A. *Gaussian 98*, revision A.9; Gaussian, Inc.: Pittsburgh, PA, 1998.

(20) Helgaker, T.; Jaszunski, M.; Ruud, K. *Chem. Rev.* **1999**, *99*, 293−352.

(21) Labastie, P.; Whetten, R. L.; Cheng, H.-P.; Holczer, K. Unpublished results. The D_2-C_{76+4m} Fullerenes: Construction of a series of intrisically helical molecules.

(22) Dresselhaus, M. S.; Dresselhaus, G.; Eklund, P. C. *Science of Fullerenes and Carbon Nanotubes*; Academic Press: San Diego, CA, 1995.

(23) Fowler, P. W.; Manolopoulos, D. E.; Batten, R. C. *J. Chem. Soc., Faraday Trans.* **1991**, *87*, 3103.

(24) Fowler, P. W. *J. Chem. Soc., Faraday Trans.* **1990**, *86*, 2073.

(25) Fowler, P. W. *J. Phys. Chem. Solids* **1993**, *12*, 1825.

(26) Van Lier, G.; Van Alsenoy, C.; Van Doren, V.; Geerlings, P. *Chem. Phys. Lett.* **2000**, *326*, 181.

(27) Fowler, P. W.; Ceulemans, A. *J. Phys. Chem.* **1995**, *99*, 508.

(28) Manolopoulos, D. E.; Woodall, D. R.; Fowler, P. W. *J. Chem. Soc., Faraday Trans.* **1992**, *88*, 2427.

(29) Fowler, P. W.; Pisanski, T. *J. Chem. Soc., Faraday Trans.* **1994**, *90*, 2865.

(30) De Proft, F.; Geerlings, P. *Chem. Rev.* **2001**, *101*, 1451.

(31) Zhou, Z. X.; Parr, R. G.; Garst, J. F. *Tetrahedron Lett.* **1988**, *29*, 4843.

(32) Zhou, Z. X.; Parr, R. G. *J. Am. Chem. Soc.* **1989**, *111*, 7371.

(33) Zhou, Z. X.; Parr, R. G. *J. Am. Chem. Soc.* **1990**, *112*, 5720.

(34) Balawender, R.; Komorowski, L.; De Proft, F.; Geerlings, P. *J. Phys. Chem. A* **1998**, *102*, 9912.

(35) Chermette, H. *J. Comput. Chem.* **1999**, *20*, 129.
(36) Geerlings, P.; De Proft, F.; Langenaeker, W. *Adv. Quantum Chem.* **1999**, *33*, 303.
(37) Geerlings, P.; De Proft, F. *Int. J. Quantum Chem.* **2000**, *80*, 227.
(38) Aihara, J. *Phys. Chem. Chem. Phys.* **2000**, *2*, 3121.
(39) London, F. *J. Phys. Radium* **1937**, *8*, 397.
(40) Steiner, E.; Fowler, P. W.; Jenneskens, L. W.; Acocella, A. *Chem. Commun.* **2001**, 659.
(41) Bühl, M.; Hirsch, A. *Chem. Rev.* **2001**, *101*, 1153.
(42) Dias, J. R. *J. Chem. Inf. Comput. Sci.* **1999**, *39*, 144.